Transport of Simple Fluids in Nanopores: Theory and Simulation

Suresh K. Bhatia and David Nicholson
Division of Chemical Engineering, The University of Queensland, Brisbane, QLD 4072, Australia

DOI 10.1002/aic.10580
Published online September 1, 2005 in Wiley InterScience (www.interscience.wiley.com).

A theory is discussed of single-component transport in nanopores, recently developed by Bhatia and coworkers. The theory considers the oscillatory motion of molecules between diffuse wall collisions, arising from the fluid–wall interaction, along with superimposed viscous flow due to fluid–fluid interaction. The theory is tested against molecular dynamics simulations for hydrogen, methane, and carbon tetrafluoride flow in cylindrical nanopores in silica. Although exact at low densities, the theory performs well even at high densities, with the density dependency of the transport coefficient arising from viscous effects. Such viscous effects are reduced at high densities because of the large increase in viscosity, which explains the maximum in the transport coefficient with increase in density. Further, it is seen that in narrow pore sizes of less than two molecular diameters, where a complete monolayer cannot form on the surface, the mutual interference of molecules on opposite sides of the cross section can reduce the transport coefficient, and lead to a maximum in the transport coefficient with increasing density. The theory is also tested for the case of partially diffuse reflection and shows the viscous contribution to be negligible when the reflection is nearly specular. © 2005 American Institute of Chemical Engineers
AIChE J, 52: 29–38, 2006
Keywords: adsorbate transport, diffusion, molecular dynamics, nanopore, viscous flow

Introduction

Modern interest in the understanding of transport in narrow pores and confined spaces dates back to the seminal works of Knudsen[1] and Smoluchowski,[2] which appeared almost a century ago. Over this period the interest has been sustained because of the relevance of this problem to a plethora of applications in heterogeneous catalysis, gas–solid reactions, separations, and gas storage. Nevertheless, despite the long history, our understanding of the subject is still rudimentary, with models being largely semiempirical and involving adjustable parameters that cannot be independently determined.[3] More recently, however, the explosive growth in research on the development and applications of new nanomaterials, such as the MCM-41S family of periodic mesoporous silicas,[4] microporous aluminosilicates and aluminophosphates,[5] carbon nanotubes,[6] and a host of other materials[7] has led to renewed interest in the subject,[8-13] with the goal of developing tractable predictive models.

The early work of Knudsen[1] considered noninteracting systems at low density, assuming diffuse reflection of molecules colliding with the pore walls. A more refined analysis, also considering viscous effects, was later presented by Pollard and Present,[14] in their classic work extending the theory to higher densities. This approach considering noninteracting systems has been prevalent in the literature, with mechanical models for interacting systems[8,13] fast becoming intractable. The most popular of the former models is the classic dusty gas model,[15] which superposes diffusive and viscous flows, leading to the result for pure component flow in cylindrical pores

$$j_z = -\left(D_0 + \frac{r_p^2 \hat{\rho} k_B T}{8\eta}\right) \frac{\hat{\rho}}{k_B T} \nabla_z \mu \tag{1}$$

Correspondence concerning this article should be addressed to S. K. Bhatia at sureshb@cheque.uq.edu.au.

in which D_0 is a diffusion coefficient, r_p is the pore radius, and η is a mean viscosity. In Eq. 1 the quantity in parentheses represents the total diffusivity based on a chemical potential gradient driving force, and can be converted to the Fickian diffusivity upon using the Darken thermodynamic correction.[3] The diffusion coefficient D_0 is taken to be the classical Knudsen coefficient in large pores (typically >5–10 nm in diameter) and an empirical activated surface diffusivity in smaller pores. The second term in the parentheses on the right-hand side represents the contribution from viscous flow, obtained using the classical Hagen–Poiseuille model, which overlooks density gradients, and assumes a uniform pressure gradient over the pore cross section. However, in small pores density gradients can be very large, indicating a key inadequacy of the viscous component in Eq. 1. Further, we have recently shown[9,11] that it is actually the chemical potential gradient that is constant over the pore cross section rather than the pressure gradient, based on observations of equilibrium density profiles being attained during equilibrium as well as nonequilibrium molecular dynamics simulations. In actual practice, however, it is difficult to establish these basic deficiencies in the above model from experimental data because the nonideal pore shape and connectivity features of porous materials necessitate the use of adjustable parameters such as tortuosity. In addition there has been no established theory for D_0 in molecularly sized pores where the Knudsen theory, which takes no account of intermolecular interactions, is seriously inadequate.

In recent times molecular dynamics simulations have emerged as a powerful option for understanding the fundamentals of the transport in confined spaces, offering an exciting avenue for the testing and validation of new theories that overcome the above limitations, which is not readily possible experimentally. Various simulation techniques such as equilibrium molecular dynamics (EMD), nonequilibrium molecular dynamics (NEMD), and dual control volume grand canonical molecular dynamics (DCV-GCMD) have been designed and applied to probe the different mechanisms and to verify proposed models.[16,17] Contradicting prior literature claims[17,18] that the different techniques measure different contributions to the transport coefficient, work in our laboratory[9,11,19] has shown that all three techniques yield the same result, even in the presence of viscous flow, and measure the total diffusion coefficient. This agrees with other observations[20,21] of the same transport coefficient being obtained from the different methods in micropores where the viscous mechanism is insignificant.

As an improvement of the classical model given in Eq. 1 we have developed a new theory for the transport of simple fluids in nanopores[10,11] that considers Lennard–Jones (LJ) interactions. Our result is exact at low density where fluid–solid interactions dominate, which has been tested for methane. At higher density it also considers fluid–fluid interactions through a coarse-grained viscosity profile based on a local average density model[22] (LADM), in which the viscosity is evaluated at a density locally averaged over the molecular diameter, following

$$\bar{\rho}(\mathbf{r}) = \frac{6}{\pi\sigma_f^3}\int_{|\mathbf{r}'|<\sigma_f/2} \rho(\mathbf{r}+\mathbf{r}')d\mathbf{r}' \qquad (2)$$

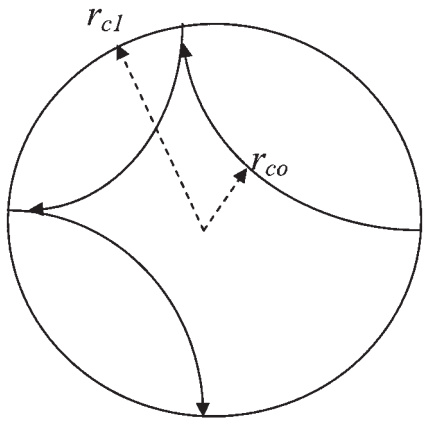

Figure 1. Schematic of trajectories of an oscillating molecule projected onto the pore cross section.

The points r_{c0} and r_{c1} represent the radial bounds of the motion, as defined in the text.

Here $\rho(\mathbf{r})$ is the density profile, σ_f is the LJ size parameter of the fluid, and $\bar{\rho}(\mathbf{r})$ is the locally averaged density. Although the theory has been tested for methane, more extensive tests with other fluids are also required to validate the theory and determine any limitations. Here, we fulfill this need, by examining the transport of H_2 and CF_4 at various pore sizes for cylindrical pores in amorphous silica at 300 K. Further, we also examine CH_4 at 300 K because in our earlier work[11] we had studied the effect of pore size with methane at 450 K. The study with hydrogen is particularly important because of the current emphasis on research for hydrogen production and storage, in anticipation of the upcoming hydrogen economy. In what follows, we first present an outline of our theory, as well as of the simulation methodology, before discussing the results and comparisons between theory and simulation.

Theory

Our theory for the transport at low density considers the motion of a fluid molecule in a cylindrical pore under the action of an axial force f, which may represent the chemical potential gradient or an applied force in NEMD simulations. In addition the molecule perceives a force field from its interaction with the pore walls, as a result of which it undergoes an oscillatory motion along the pore cross section while being axially forced by the applied force f. The radial bounds of this oscillatory motion correspond to the points where the molecule changes direction, given by the values r_{c0} and r_{c1} in Figure 1, which depicts the motion. Of these r_{c1} corresponds to the point of reflection, and at this point the molecule is assumed to be reflected diffusely in the osculating plane, thereby losing its net momentum.

Although the above diffuse reflection assumption corresponds to that used by Knudsen[1] in his classic derivation for noninteracting systems, recent simulation-based studies of diffusion of methane and hydrogen in ideal graphitic slit pores and carbon nanotubes[23-26] have shown that reflection from these surfaces can be nearly specular. Such behavior is attributable to the nearly smooth energy landscape offered by graphitic surfaces, where the interatomic spacing of the covalently bonded carbon atoms of about 0.142 nm is significantly smaller than

the size of the diffusing molecule. As shown by Arya et al.[27] the nature of the reflection is a highly sensitive function of the surface morphology and structure. Indeed, in more recent simulations reflections from carbon nanotubes with surface defects have been found to be much less specular, with a high degree of diffuse component,[28] whereas experiments with nitrogen diffusion in large carbon nanotubes (0.75 nm diameter), in which fluid–solid interactions are weak, have been satisfactorily explained based on the Knudsen diffusion coefficient.[29] These latter studies would suggest the relevance of the diffuse reflection condition to real porous materials where smooth energy landscapes would be the exception rather than the rule.

Under conditions of steady flow the transport coefficient may be determined from the mean duration $\langle\tau\rangle$ of the trajectory between successive reflections, following[10]

$$D_{t0} = \frac{k_B T}{m} \langle\tau\rangle \tag{3}$$

which conjugates with a chemical potential gradient driving force. The mean oscillation time $\langle\tau\rangle$ may be obtained by an analysis of the trajectory dynamics. To this end we define the Hamiltonian

$$H = \phi_{fs}(r) + \frac{p_r^2}{2m} + \frac{p_\theta^2}{2mr^2} + \frac{p_z^2}{2m} - zf \tag{4}$$

for the particle motion in the conservative potential field of the adsorbent, $\phi_{fs}(r)$, assumed to be one-dimensional. Here p_r, p_θ, and p_z are the momenta in cylindrical coordinates. Further, for the low-density case being solved for here, fluid–fluid interactions are considered insignificant and not considered in the Hamiltonian. Following the Hamiltonian equations of motion $dp_r/dt = -\partial H/\partial r$, $dr/dt = \partial H/\partial p_r$, we obtain the solution for the radial momentum profile of a particle moving toward the wall

$$p_r(r', r, p_r, p_\theta) = \left\{ 2m[\phi_{fs}(r) - \phi_{fs}(r')] + p_r^2(r) + \frac{p_\theta^2}{r^2}\left(1 - \frac{r^2}{r'^2}\right)\right\}^{1/2} \tag{5}$$

Here $p_r(r', r, p_r, p_\theta)$ is the radial momentum at position r' for a particle having radial momentum p_r at position r. By using the relation $mdr/dt = p_r$ Eq. 5 readily provides the oscillation time as

$$\tau(r, p_r, p_\theta) = 2m \int_{r_{c0}(r,p_r,p_\theta)}^{r_{c1}(r,p_r,p_\theta)} \frac{dr'}{p_r(r', r, p_r, p_\theta)} \tag{6}$$

where $r_{c1}(r, p_r, p_\theta)$ and $r_{c0}(r, p_r, p_\theta)$ are the values of r' corresponding to the solution of

$$p_r(r', r, p_r, p_\theta) = 0 \tag{7}$$

Considering a canonical distribution of energies we may now obtain the mean oscillation time, and subsequently the transport diffusivity at low density, following Eq. 3, as

$$D_{t0}^{LD} = \frac{2}{\pi m Q} \int_0^\infty e^{-\beta\phi_{fs}(r)} dr \int_0^\infty e^{-\beta p_r^2/2m} dp_r \times \int_0^\infty e^{-\beta p_\theta^2/2mr^2} dp_\theta \int_{r_{c0}(r,p_r,p_\theta)}^{r_{c1}(r,p_r,p_\theta)} \frac{dr'}{p_r(r', r, p_r, p_\theta)} \tag{8}$$

where $Q = \int_0^\infty re^{-\beta\phi_{fs}(r)} dr$ and $p_r(r', r, p_r, p_\theta)$ follows Eq. 5. This result is valid under conditions at which intermolecular interactions between the moving fluid particles are insignificant.

At higher densities where fluid–fluid interactions cannot be ignored, viscous effects become significant, and are approximated by using the LADM discussed above in a Navier–Stokes framework. For this we solve the equation of motion in cylindrical geometry

$$\frac{1}{r}\frac{d}{dr}\left[r\eta(r)\frac{du_z}{dr}\right] = \rho(r)\frac{d\mu}{dz} \tag{9}$$

obtained by combining the Navier–Stokes and Gibbs–Duhem equations.[19] Here $\rho(r)$ is the density profile and $\eta(r)$ is the local viscosity obtained at the local average density $\bar{\rho}(r)$, defined through Eq. 2. By consideration of uniform chemical potential along the pore cross section and a no-slip boundary condition, the solution of Eq. 9 yields the viscous contribution to the transport coefficient

$$D_{t0}^{vis}(\hat{\rho}) = \frac{2k_B T}{\hat{\rho} r_p^2} \int_0^{r_0} \frac{dr}{r\eta[\bar{\rho}(r)]} \left(\int_0^r r'\rho(r')dr' \right)^2 \tag{10}$$

where r_p is the pore radius, and we have used the phenomenological relation

$$j_z = \frac{D_{to}\hat{\rho}}{k_B T}(-\nabla\mu) \tag{11}$$

for the pore flux j_z. Here $\hat{\rho}$ is the overall pore density. Further, r_0 is the position of the potential energy minimum, at which point the no-slip condition has been applied. Molecules crossing this location while moving toward the wall will be rapidly decelerated and reflected.

To correct for the surface slip we use the low-density transport coefficient in Eq. 8, and the approximation

$$D_{t0}(\hat{\rho}) = D_{t0}^{LD} + D_{t0}^{vis}(\hat{\rho}) \tag{12}$$

to provide the overall transport coefficient, in analogy with the superposition of diffusive and viscous contributions in Eq. 1. Although not rigorously obtained here such a superposition is naturally obtained in theories based on momentum transfer arguments.[19]

Simulation

As discussed earlier preliminary validation of the above approach has been made using only methane, over a narrow range of conditions. These covered a range of pore sizes at 450 K, and various temperatures at pore diameter of 3.01 nm. Here we apply the theory to H_2, CF_4, and CH_4 at 300 K, covering a wide range of pore sizes (0.65–5.39 nm). Each of these molecules is treated as an LJ fluid, with parameters as specified in Table 1 for the different species. The pore walls are assumed amorphous and infinitely thick, and composed of closely packed LJ sites having parameters[19] $\varepsilon_s/k_B = 290$ K, $\sigma_s = 0.29$ nm, and spaced $2^{1/6}\sigma_s$ apart. The one-dimensional fluid–solid potential at any position is obtained by summing over the interaction of an LJ methane particle at that position with sites lying up to five atomic diameters on either side. The Lorentz–Berthelot rules are applied to estimate fluid–solid LJ parameters, and a total of 12 layers of sites in the pore wall are used in the summation. A cutoff distance of 1.5 nm is used in estimating fluid–fluid interactions for CH_4 and H_2 and 2.5 nm for CF_4.

Equilibrium molecular dynamics simulations were conducted as detailed earlier,[11] and collective transport coefficients obtained from the autocorrelation of the streaming velocity of the system by a Green–Kubo relation

$$D_{t0} = N \lim_{\tau\to\infty} \int_0^\tau \langle u_z(0)u_z(t)\rangle dt \tag{13}$$

where

$$u_z(t) = \frac{1}{N}\sum_{i=1}^{N}\frac{dz_i}{dt} = \frac{1}{N}\sum_{i=1}^{N} v_{iz}(t) \tag{14}$$

is the instantaneous axial streaming velocity. The EMD was initiated from an initial configuration generated by grand canonical Monte Carlo simulation (GCMC), and typically the pore had about 500 particles in the EMD simulation. The run length was typically 10^7 time steps, and each time step was 0.5 fs for H_2, 1 fs for CH_4, and 2 fs for CF_4. A Gaussian thermostat[30] was used to control the temperature during the simulation. This thermostat introduces a viscous damping into the equation of motion so as to *rigidly* keep the kinetic energy constant based on the required temperature. From the perspective of testing the theory the Gaussian thermostat would therefore appear the most appropriate, even if not as realistic as others,[16] that have weaker damping and allow larger temperature fluctuations. Further, a diffuse reflection condition was applied whenever a molecule changed direction, after having crossed the potential minimum location when moving toward the pore wall.

Table 1. LJ Potential Parameters for Various Fluids

Fluid Parameter	H_2	CH_4	CF_4
σ_{ff} (nm)	0.2915	0.381	0.4662
ε_{ff}/k_B (K)	38.0	148.1	134.0

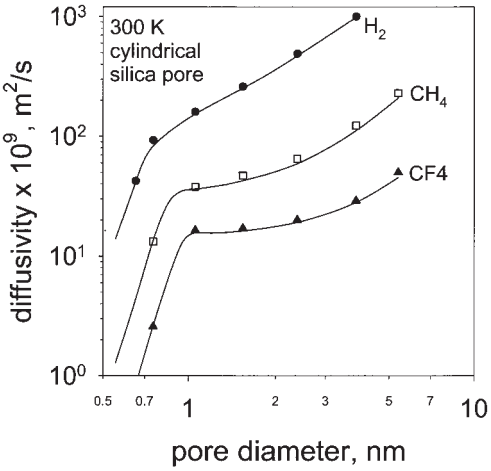

Figure 2. Comparison of simulation and predicted variation of low-density transport coefficient with pore diameter for the three gases at 300 K.

Symbol: simulation values; lines: theoretical results.

Results and Discussion

Low-density transport

At low densities, intermolecular interactions in the fluid can be neglected and Eq. 8 provides the transport coefficient. In the current work we investigated the transport of the chosen gases at 300 K, at pore diameters of 0.65, 0.75, 1.05, 1.54, 2.39, 3.84, and 5.39 nm. Figure 2 illustrates the comparison between theory and simulation, showing excellent agreement for all three gases, with the theory being essentially exact. Although detailed error bars are not shown here, our estimates showed the simulation errors to be within 5%, as obtained from four to five runs at densities $\lesssim 0.5$ nm^{-3}, for each gas.

An interesting feature of Figure 2 is the steep slope of the variation of diffusivity with pore size, at small pore diameter, for all species. For hydrogen ($\sigma_f = 0.2915$ nm) this occurs below about 0.75 nm; for CH_4 ($\sigma_f = 0.381$ nm) this occurs below about 0.9 nm diameter; whereas for the much larger molecule CF_4 ($\sigma_f = 0.4662$ nm) this occurs below about 1.05 nm diameter. For pore sizes below the corresponding pore size for each gas the diffusivity diminishes drastically with pore size, suggesting the origin of kinetic molecular sieving behavior. At the critical pore size for each gas the ratio of molecular size σ_f to open pore diameter ($2r_p - \sigma_s$) is about 0.61–0.63, and the molecules are no longer confined to the pore axis.

Figure 3 depicts the potential energy profile for hydrogen, showing the peak to lie at the pore center for a pore of diameter 0.65 nm, and slightly off-center, with increased width, for a pore of diameter 0.75 nm. Similarly for CF_4 the peak lies off-center at a pore diameter of 1.05 nm, somewhat closer to the center at a pore diameter of 0.95 nm, and at the center for a pore diameter of 0.85 nm, as shown in Figure 4. Because at low density the molecules are localized at the position of the potential energy minimum, for molecules large enough that the potential energy minimum is at the center, the frequency of collisions with the pore surface will be significantly increased with decrease in pore diameter, and on the grounds of Eq. 3 the diffusivity will correspondingly decrease. On the other hand, for molecules that are localized only slightly off-center, the

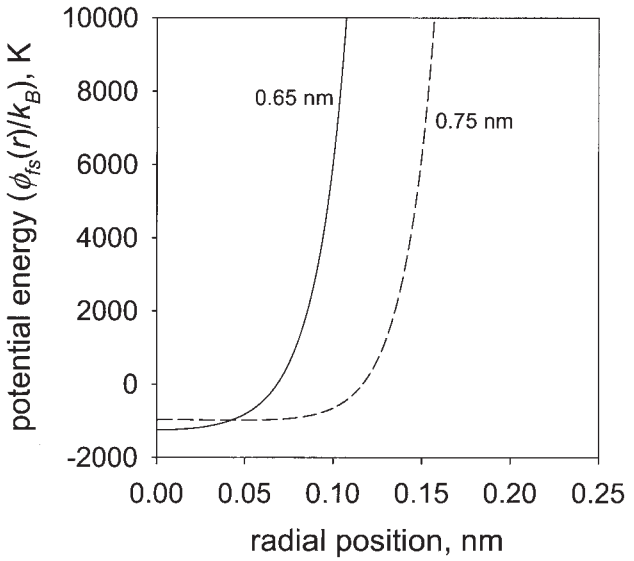

Figure 3. Potential energy profiles for hydrogen in pores of 0.65 and 0.75 nm diameter.

trajectories will be considerably longer and the time between reflections will therefore be correspondingly larger, leading to appreciably higher diffusivities. Thus, in this way the present theory provides a mechanistic explanation of kinetic molecular sieving. A related phenomenon, known as a "levitation " or "floating molecule " effect, has been observed in simulations for molecules passing through windows between zeolite cages.[31-33]

It was previously shown[11] that for noninteracting systems Eq. 8 leads exactly to the traditional Knudsen result. For the systems examined here, however, interactions are not negligible because it is readily estimated that the diffusivity values

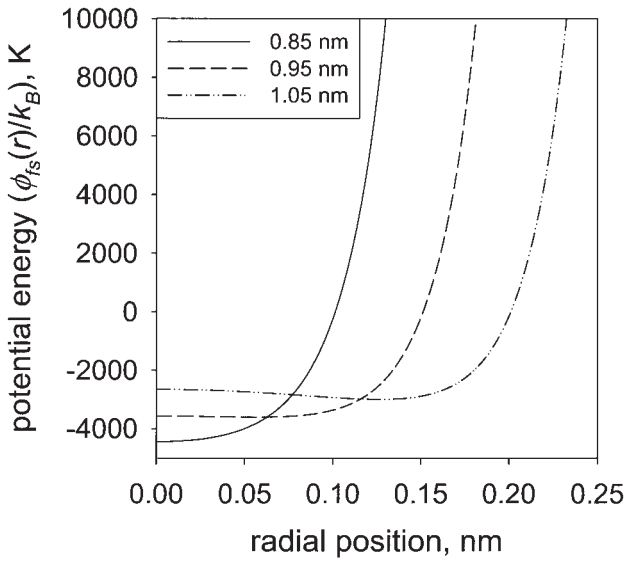

Figure 4. Potential energy profiles for carbon tetrafluoride in pores of 0.85, 0.95, and 1.05 nm diameter.

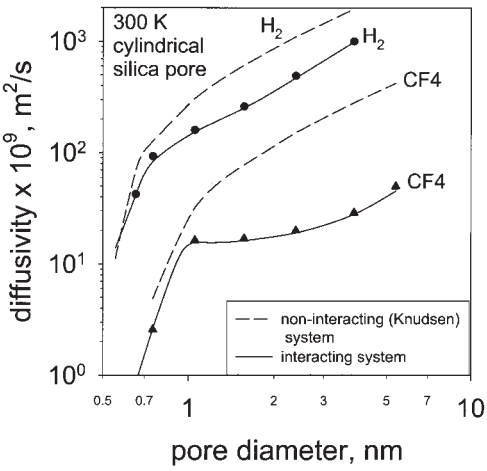

Figure 5. Comparison of transport coefficient dependency on pore diameter, for interacting and noninteracting systems.

Symbols: simulation values; lines: theoretical results.

depicted in Figure 2 are significantly smaller than those predicted by the corrected Knudsen expression

$$D_{i0}^{LD} = \frac{4r_{ph}}{3}\sqrt{\frac{2k_BT}{\pi m}} \tag{15}$$

in which the pore radius r_{ph} represents the distance between the pore center and of the adsorptive at the point of reflection, assuming a noninteracting (that is, hard sphere system). Figure 5 compares the variation of the Knudsen diffusivity with pore diameter $2r_p$ (pore radius r_p = distance of the centers of the surface adsorbent atoms from the pore center), assuming $r_{ph} = r_p - 0.92\sigma_{fs}$, with the results for the more realistic interacting system, for H_2 and CF_4. The classical Knudsen assumption, that the molecules do not interact with the wall (apart from a diffuse hard sphere reflection), substantially overestimates the diffusion, and the corrected Knudsen diffusivity is as much as 10 times larger for CF_4 for a pore diameter of 3.84 nm. For the more weakly adsorbing hydrogen the overestimation is somewhat less, but still as much as 2.3 at a pore diameter of 1.57 nm.

This overestimation by the Knudsen equation is attributed to the neglect of dispersive fluid–wall interactions, given that the latter serve to slow the moving molecules after reflection and shorten the trajectories between collisions. The neglect of these interactions in the Knudsen theory thus leads to longer trajectories, thereby increasing the value of the mean oscillation period $\langle\tau\rangle$, which increases the overall transport coefficient. The modification of the trajectories arising from wall–fluid forces has been noted in an early numerical study of molecular flow in narrow spaces,[34] although the effect on the oscillation period and the relation with the transport coefficient are unique to the current theory. The Knudsen diffusion coefficient is routinely used in analysis of adsorption kinetics and in the calculation of effectiveness factors in porous catalysts, and the present results suggest that considerable error is encountered in such an approach in small pores, where the dispersive interactions are significant.

The model as developed is valid for a simple fluid composed

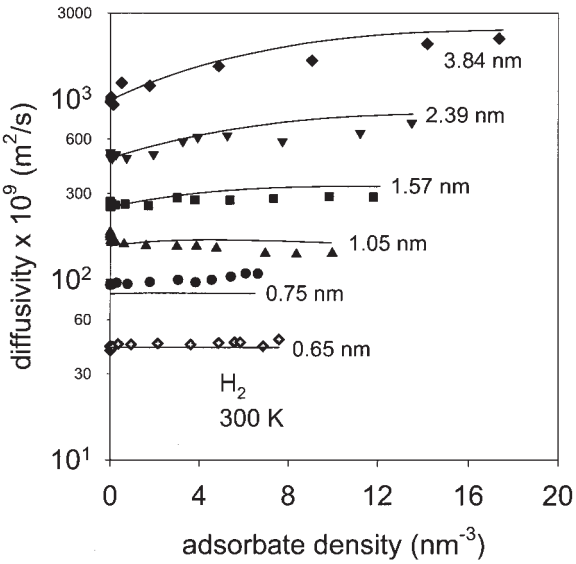

Figure 6. Variation of transport coefficient with density, for hydrogen in pores of various diameters.

Symbols: simulation values; lines: theoretical results.

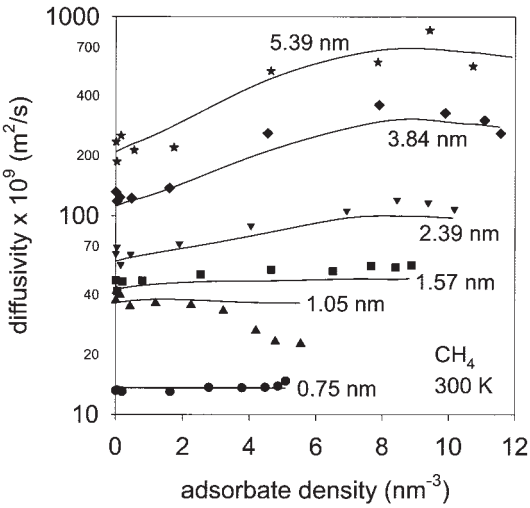

Figure 7. Variation of transport coefficient with density, for methane in pores of various diameters.

Symbols: simulation values; lines: theoretical results.

of Lennard–Jones particles. The extension to a molecule of multiatom particles would appear to be a natural area of extension of the present approach. Although possible in principle, the computational burden is likely to be increased manifold because rotational degrees of freedom would add integrals over at least four additional dimensions (two angular dimensions and corresponding angular momenta for a linear molecule), making the approach computationally cumbersome even in comparison to MD simulation.

Transport at finite density

Following the above results for low-density EMD, simulations were performed for the transport at finite density, for each of the three gases in pores of various diameters at 300 K. In addition, Eqs. 8, 10, and 12 were used to estimate the theoretical transport coefficient, for comparison with the simulation results. For the theoretical predictions the density profile was taken as the equilibrium profile, which was obtained from GCMC simulation. As discussed earlier, the validity of the equilibrium profile during transport has been confirmed in our earlier studies[9,11,19] and, although obtained here by GCMC simulation, the same may also be obtained theoretically by means of density functional theory. The theoretical calculations also require the estimation of the viscosity profile, evaluated based on the locally averaged density profile obtained using Eq. 2. For this, the viscosity at the local average density was obtained using an adaptation of the Enskog method to finite density following Mehdipour and Eslami.[35] Figures 6–8 depict the results obtained for the three different gases, and the comparison with simulation. As before, the uncertainty of the simulation results is about 5%, as obtained from repeat simulations at selected densities. As seen in the figures the theory can predict the transport coefficient satisfactorily over the range of pore sizes studied, although for CF_4 some underprediction is evident at the larger pore diameters of 3.84 and 5.39 nm. Although this deviation may well be a result of errors arising from the LADM approximation, the accuracy of the viscosity estimation method needs to be verified before such a conclusion can be made. Our searches did not reveal any widely accepted method for the prediction of the bulk viscosity for Lennard–Jones fluids.

In our earlier studies[9,11,19] we used the viscosity correlation of Chung et al.[36]; however, this requires critical property data rather than LJ parameters, and it was therefore decided to adopt a method more appropriate for an LJ fluid. The results are only marginally different from those obtained using the Chung et al.[36] correlation. Although alternate correlations such as those of Rowley and Painter[37] and of Zabaloy et al.[38] exist they were found to be highly inaccurate for hydrogen and therefore unsuitable for the present study. Another approach may be to

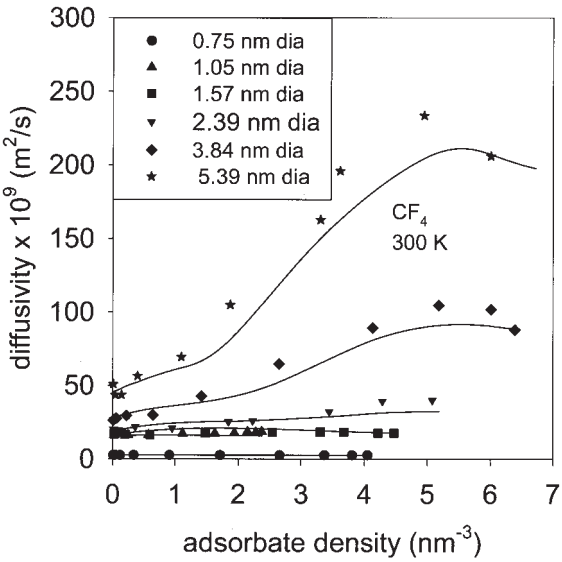

Figure 8. Variation of transport coefficient with density, for CF_4 in pores of various diameters.

Symbols: simulation values; lines: theoretical results.

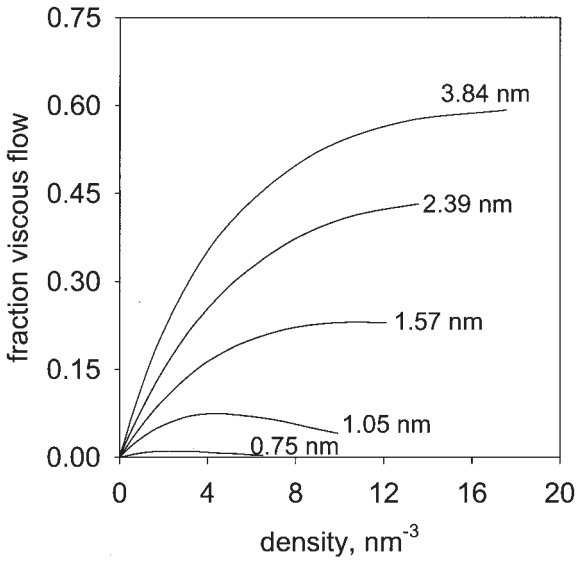

Figure 9. Density variation of fractional contribution of viscous flow to the total transport coefficient for hydrogen, in pores of various diameters, at 300 K.

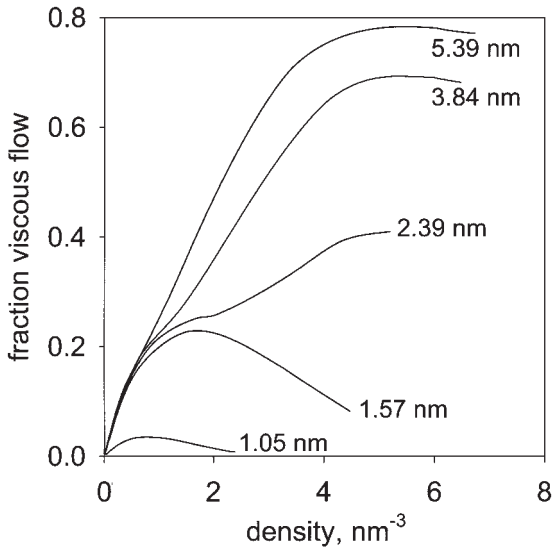

Figure 11. Density variation of fractional contribution of viscous flow to the total transport coefficient for CF_4, in pores of various diameters, at 300 K.

compute the bulk viscosity as a function of density using EMD or NEMD simulation for the bulk fluid and this will be examined in the future, although it detracts from the simplicity and computational convenience of a viscosity correlation.

Figures 6–8 show a strong density dependency of the transport coefficient, based on simulation as well as theory. As seen from Eq. 12 this density dependency arises in the theory from the viscous part, and with increasing density the transport coefficient generally increases except for very high densities where a decrease is evident. The importance of viscous transport at finite densities is shown in Figures 9–11, illustrating the

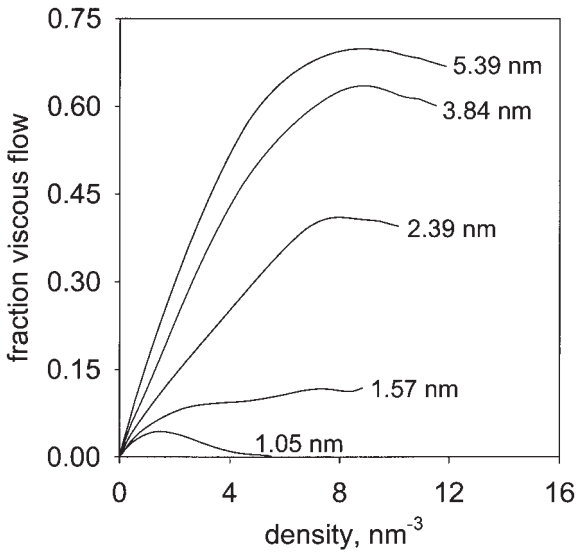

Figure 10. Density variation of fractional contribution of viscous flow to the total transport coefficient for methane, in pores of various diameters, at 300 K.

predicted fractional viscous contribution to the total transport coefficient as a function of density at the various pore sizes, for the three gases studied herein. These figures show the viscous fraction to be very significant for pore size of $\geq$1.57 nm, for all three gases, exceeding even 60% at the largest pore diameter studied. With increasing pore size the viscous fraction increases, as expected. However, for large pore sizes at high densities the viscous fraction appears to reduce with increasing density for CH_4 and CF_4, consistent with the decrease in transport coefficient indicated above. Thus, for methane the transport coefficient reduces with increasing density $\gtrsim$ 8.5 nm^{-3}, for pore diameters of $\geq$2.39 nm, whereas for CF_4 this occurs at a density $\gtrsim$ 5.5 nm^{-3}, for pore diameters of $\geq$3.84 nm. This decrease results from the high sensitivity of the bulk viscosity to density at these high densities for methane and CF_4, as shown in Figure 12, based on the viscosity estimation method used.[35] For hydrogen the viscosity is relatively less sensitive to density over the range of densities studied and the transport coefficient does not decrease in this range, as seen in Figure 6.

It is also notable that for small pore size in the micropore range the viscous fraction decreases with increasing density, at relatively low density. This occurs, for example, for pore diameter of 1.05 nm for all gases, and at this pore size the transport coefficient for methane also shows a large decline with increase in density, after an initial region of almost constant diffusivity. This decline is explained by the interaction between diametrically opposite molecules, given that a complete monolayer cannot form at this pore size. Such interactions lead to more frequent reflections and shorter oscillation period of the molecules, which reduces the transport coefficient on the basis of Eq. 3. Such effects are not well captured in the LADM approach on which the viscous term in Eq. 12 is based, leading to the predictive error in this region of rapid decline of the transport coefficient. Theoretical improvements in this region are therefore needed and will be examined in the future.

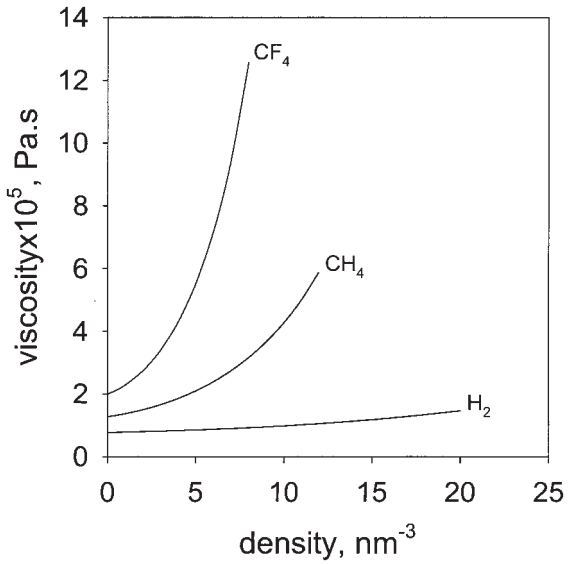

Figure 12. Variation of bulk viscosity with density at 300 K.

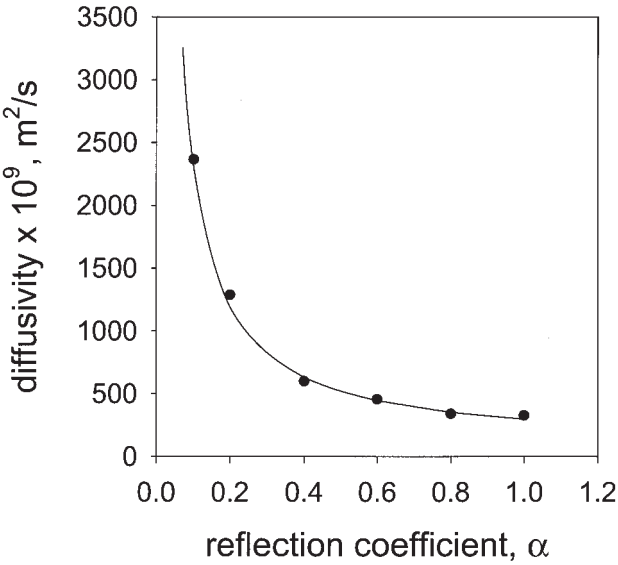

Figure 13. Variation of diffusion coefficient of methane with fraction of collisions having diffuse reflection, in a pore of 3.848 nm diameter at 300 K.

Symbols: simulation data; curve: theoretical result.

Effect of departure from diffuse reflection

As discussed earlier there has been some discussion in the literature regarding the nature of the reflection when a fluid atom collides with the solid surface. Although we have used the diffuse reflection condition here, fully atomistic simulations[23-26] in carbon nanotubes and slit pore carbons having an ideal graphitic surface structure suggest nearly specular reflection in these cases. Nevertheless, depending on the surface texture and morphology the reflections can span the entire range between specular and diffuse.[27,28] Consequently, it is instructive to consider the effect of only partially diffuse reflection on the transport. To this end we may use the classical model that a fraction α of the collisions is diffuse and the remainder is specular. An alternative model[12] considers that each reflection constitutes both diffusive and specular components in a fixed ratio. However, both are effective representations in that individual collisions are influenced by the local morphology of the surface and the extent of diffuse reflection will therefore not be uniform[26]; thus there is no obvious choice regarding the model used.

Considering that a fraction α of the collisions is diffuse, the low-density transport coefficient is given by[20,35]

$$D_{t0}(\hat{\rho} = 0) = \frac{(2 - \alpha)}{\alpha} D_{t0}^{LD} \tag{16}$$

where D_{t0}^{LD} follows Eq. 8. The factor $(2 - \alpha)/\alpha$ is identical to the familiar Smoluchowski[2] correction for deviation from diffuse reflection, originally derived for noninteracting systems, but derived[20,39] in our case for interacting systems. By incorporating the viscous contribution in a manner analogous to that in Eq. 12, we obtain

$$D_{t0}(\hat{\rho}) = \frac{(2 - \alpha)}{\alpha} D_{t0}^{LD} + D_{t0}^{vis}(\hat{\rho}) \tag{17}$$

where the viscous term follows Eq. 10. Equation 17 has recently been used[26] to determine the reflection coefficient α, for hydrogen and methane diffusion in carbon nanotubes, from values of the transport coefficient determined by atomistic simulations. The values of α so determined were in good agreement with those determined directly from simulation,[24] confirming the applicability of the theory. As another test of the theory, here we have conducted simulations, as described earlier, for methane at 300 K and an adsorbed density of 9.9 nm^{-3} in a 3.84 nm diameter silica pore, with the diffuse reflection condition being replaced by one in which only a random fraction α of the reflections is diffuse. These simulations used a nonequilibrium molecular dynamics (NEMD) method,[16,17,19] in which a constant acceleration is applied to the fluid atoms, in place of the EMD technique discussed earlier. Figure 13 depicts the comparison of simulation and theory in this case, validating the result in Eq. 17. The figure also shows the steep increase in transport coefficient at small α, resulting from the singularity in Eq. 17 as $\alpha \to 0$. This singularity arises because in the case of specular reflection (that is, $\alpha = 0$) there is no momentum loss on reflection of a fluid atom, and therefore no net force at the wall that opposes the applied chemical potential gradient driving force. Consequently there is a force imbalance on the fluid and steady state cannot be achieved, as a result of which the transport coefficient becomes unbounded.

Figure 14 depicts calculation results for the variation of normalized diffusivity and viscous fraction with α, for methane at 300 K in a pore of 3.84 nm diameter at various densities, based on Eq. 17, with D_{t0}^{LD} and the viscous contribution $D_{t0}^{vis}(\hat{\rho})$, following Eqs. 8 and 10, respectively. As in Figure 13 we note the steep increase in diffusivity with decrease in α, at small α, for all the densities examined, with a more than 100-fold increase by $\alpha = 0.01$. At the same time the fraction of viscous flow shows an opposite trend and increases almost

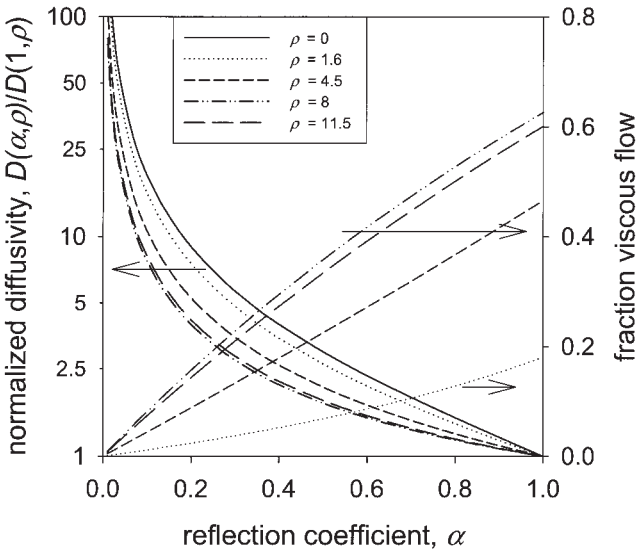

Figure 14. Theoretical variation of normalized diffusivity with reflection coefficient α, for methane transport in a pore of 3.84 nm diameter, at 300 K and various densities.

linearly with α. At small α the diffusive contribution clearly dominates, ascribed to the factor $(2 - \alpha)/\alpha$ in the first term of Eq. 17, and the viscous fraction approaches zero. Thus in transport in pores with nearly specular surfaces, such as in carbon nanotubes, the viscous contribution will be negligible, as highlighted in a recent study.[26]

Conclusions

In this article we have further tested a recent theory from the first author's laboratory on the transport of Lennard–Jones fluids in nanopores. The theory combines a model of molecular oscillations along the pore cross section with a viscous flow model, accounting for the strong density profile in nanopores. Comparisons between theoretical and equilibrium molecular simulation–based transport coefficients have been made for hydrogen, methane, and carbon tetrafluoride in cylindrical silica pores of various diameters. At low densities, where viscous flow is negligible, the theory is found to be exact and provides excellent agreement with simulation in all cases. The theory also provides an explanation of the kinetic molecular sieving between closely sized molecules, based on the large sensitivity of diffusivity to pore size when the pore and molecular size are very close. The density variation of the transport coefficient is represented in the theory in terms of viscous flow, based on a local average density model, which satisfactorily explains the simulation results. At high density some deviation between theory and simulation is seen, particularly for carbon tetrafluoride, which may be related to inaccuracies in the bulk viscosity correlation used. Further, substantial sensitivity of the bulk viscosity to density at high densities can lead to a decrease in viscous flow and therefore the transport coefficient at high densities, which is found to explain the maximum in simulation-based transport coefficients. The theory also proved to be adequate when the wall reflection is only partially diffuse, showing the viscous contribution to be insignificant for flow in pores with nearly specular surfaces.

Acknowledgments

This research was supported by a grant from the Australian Research Council under the Discovery scheme.

Literature Cited

1. Knudsen M. Die Gesetze der Molekularströmung und der inneren Reibungsströmung der Gase durch Röheren. *Ann Phys* (*Leipzig*) 1909; 28:75-130.
2. Smoluchowski von MV. Zur Kinetischen Theorie der Transpiration und Diffusion verdünnter Gase. *Ann Phys* (*Leipzig*) 1910;33:1559-1570.
3. Kärger J, Ruthven DM. *Diffusion in Zeolites and Other Microporous Solids.* New York, NY: Wiley; 1992.
4. Selvam P, Bhatia SK, Sonwane CG. Recent advances in processing and characterization of periodic mesoporous MCM-41 silicate molecular sieves. *Ind Eng Chem Res.* 2001;40:3237-3261.
5. Davis ME. Zeolites and molecular sieves: Not just ordinary catalysts. *Ind Eng Chem Res.* 1991;30:1675-1691.
6. Saito R, Dresselhaus G, Dresselhaus MS. *Physical Properties of Carbon Nanotubes.* London, UK: Imperial College Press; 1998.
7. Davis ME. Ordered porous materials for emerging applications. *Nature.* 2002;417:813-821.
8. Pozhar LA, Gubbins KE. Transport properties of inhomogeneous fluid mixtures. *Int J Thermophys.* 1999;20:805-813.
9. Bhatia SK, Nicholson D. Hydrodynamic origin of diffusion in nanopores. *Phys Rev Lett*. 2003;90:016105.
10. Jepps OG, Bhatia SK, Searles DJ. Wall mediated transport in confined spaces: Exact theory for Lennard–Jones fluids. *Phys Rev Lett*. 2003; 91:0126102.
11. Bhatia SK, Jepps OG, Nicholson D. Tractable molecular theory of transport of Lennard–Jones fluids in nanopores. *J Chem Phys.* 2004; 120:4472-4485.
12. Arya G, Chang H-C, Maginn EJ. Knudsen diffusivity of a hard sphere in a rough slit pore. *Phys Rev Lett*. 2003;91:026102.
13. Davis HT. In: Henderson D, ed. Kinetic theory of strongly inhomogeneous fluids. *Fundamentals of Inhomogeneous Fluids*. New York, NY: Marcel Dekker; 1992.
14. Pollard WG, Present RD. On gaseous self-diffusion in long capillary tubes. *Phys Rev* 1948;73:762-773.
15. Mason EA, Malinauskas AP, Evans RB. Flow and diffusion of gases in porous media. *J Chem Phys* 1967;46:3199-3216.
16. Allen MP, Tildesley DJ. *Computer Simulation of Liquids.* Oxford, UK: Clarendon; 1987.
17. Nicholson D, Travis KP. In: Kanellopoulos N, ed. Molecular simulation of transport in a single micropore. *Recent Advances in Gas Separation by Microporous Membranes*. Amsterdam, The Netherlands: Elsevier; 2000.
18. Travis KP, Gubbins KE. Combined diffusive and viscous transport of methane in a carbon slit pore. *Mol Simul.* 2000;25:209-227.
19. Bhatia SK, Nicholson D. Molecular transport in nanopores. *J Chem Phys.* 2003;119:1719-1730.
20. Jepps OG, Bhatia SK, Searles DJ. Modelling diffusion transport in slit pores. *J Chem Phys.* 2004;120:5396-5406.
21. Arya G, Chang HC, Maginn E. A critical comparison of equilibrium, non-equilibrium and boundary-driven molecular dynamics techniques for studying transport in microporous materials. *J Chem Phys.* 2001; 115:8112-8124.
22. Bitsanis I, Vanderlick TK, Tirrell M, Davis HT. A tractable molecular theory of flow in strongly inhomogeneous fluids. *J Chem Phys*. 1988; 89:3152.
23. Sokhan VP, Nicholson D, Quirke N. Fluid flow in nanopores: An examination of hydrodynamic boundary conditions. *J Chem Phys*. 2001;115:3878-3887.
24. Sokhan VP, Nicholson D, Quirke N. Fluid flow in nanopores: Accurate boundary conditions for carbon nanotubes. *J Chem Phys*. 2002;117: 8531-8539.
25. Chen HB, Sholl DS. Rapid diffusion of CH_4/H_2 mixtures in single-wall carbon nanotubes. *J Am Chem Soc*. 2004;126:7778-7779.

26. Bhatia SK, Chen HB, Sholl DS. Comparisons of diffusive and viscous contributions to transport coefficients of light gases in single-walled carbon nanotubes. *Mol Simul*. 2005;31:643-649.
27. Arya G, Chang H-C, Maginn EJ. Molecular simulations of Knudsen wall-slip: Effect of wall morphology. *Mol Simul*. 2003;29:697-709.
28. Roth MW, Mesentseva J. Atomistic simulations of rare gas transport through breathable single-wall nanotubes with constrictions and knees. *Mol Simul*. 2004;30:661-667.
29. Hinds BJ, Chopra N, Rantell T, Andrews R, Gavalas V, Bachas LG. Aligned multiwalled carbon nanotube membranes. *Science.* 2004;303: 62-65.
30. Evans DJ, Morriss GP. *Statistical Mechanics of Nonequilibrium Liquids.* London, UK: Academic Press; 1990.
31. Derouane EG, Andre J-M, Lucas AA. Surface curvature effects in physisorption and catalysis by microporous solids and molecular-sieves. *J Catal*. 1988;110:58-73.
32. Yashonath S, Santikary P. Diffusion of sorbates in zeolite-y and zeolite-a—Novel dependence on sorbate size and strength of sorbate–zeolite interaction. *J Phys Chem.* 1994;98:6368-6376.
33. Bandyopadhyay S, Yashonath SJ. Diffusion anomaly in silicalite and vpi-5 from molecular-dynamics simulations. *Phys Chem*. 99:4286-4292.
34. Nicholson D, Petropoulos JH. A fundamental approach to molecular flow in pore spaces. *Ber Bunsen-Ges Phys Chem*. 1975;79:796-798.
35. Mehdipour N, Eslami H. Calculation of transport properties of simple dense fluids. *Int J Thermophys*. 2002;41:949-954.
36. Chung TH, Ajlan M, Lee LL, Starling KE. Generalized multiparameter correlation for nonpolar and polar fluid transport-properties. *Ind Eng Chem Res*. 1988;27:671-679.
37. Rowley RL, Painter MM. Diffusion and viscosity equations of state for a Lennard–Jones fluid obtained from molecular dynamics simulations. *Int J Thermophys*. 1997;18:1109-1121.
38. Zabaloy MS, Machado JMV, Macedo EA. A study of Lennard–Jones equivalent analytical relationships for modeling viscosities. *Int J Thermophys.* 2001;22:829-858.
39. Jepps O, Bhatia SK, Searles DJ. Effects of the juxtaposition of carbonaceous slit-pores on the overall transport behaviour of adsorbed fluid. *Langmuir.* 2005;21:229-239.

Manuscript received Feb. 8, 2005, and revision received May 8, 2005.